Manuscript prepared for The Cryosphere
with version 2016/01/22 8.09 Copernicus papers of the LATEX class copernicus.cls.
Date: 16 May 2016

Application and validation of long-range terrestrial laser scanning to monitor the mass balance of very small glaciers in the Swiss Alps

Mauro Fischer[1], Matthias Huss[1,2], Mario Kummert[1], and Martin Hoelzle[1]

[1]Department of Geosciences, University of Fribourg, 1700 Fribourg, Switzerland
[2]Laboratory of Hydraulics, Hydrology and Glaciology (VAW), ETH Zurich, 8093 Zurich, Switzerland

Correspondence to: Mauro Fischer (mauro.fischer@unifr.ch)

Abstract. Due to the relative lack of empirical field data, the response of very small glaciers (here defined as being smaller than $0.5\,\mathrm{km}^2$) to current atmospheric warming is not fully understood yet. Investigating their mass balance, e.g., using the direct glaciological method, is a prerequisite to fill this knowledge gap. Terrestrial laser scanning (TLS) techniques operating in the near infrared range can be applied for the creation of repeated high-resolution digital elevation models and consecutive derivation of annual geodetic mass balances of very small glaciers. This method is promising, as laborious and potentially dangerous field measurements as well as the inter- and extrapolation of point measurements can be circumvented. However, it still owes to be validated. Here, we present TLS-derived annual surface elevation and geodetic mass changes for five very small glaciers in Switzerland (Glacier de Prapio, Glacier du Sex Rouge, St. Annafirn, Schwarzbachfirn, and Pizolgletscher) and two consecutive years (2013/14–2014/15). The scans were acquired with a long-range *Riegl* VZ-6000 especially designed for surveying snow- and ice-covered terrain. Zonally variable conversion factors for firn and bare ice surfaces were applied to convert geodetic volume to mass changes. We compare the geodetic results to direct glaciological mass balance measurements coinciding with the TLS surveys and assess the uncertainties and errors included in both methods. Average glacier-wide mass balances were negative in both years, showing stronger mass losses in 2014/15 (–1.65 m w.e.) compared to 2013/14 (–0.59 m w.e.). Geodetic mass balances were slightly less negative but in close agreement with the direct glaciological ones ($R^2 = 0.91$). Due to the dense in-situ measurements, the uncertainties in the direct glaciological mass balances were small compared to the majority of measured glaciers worldwide (± 0.09 m w.e. yr^{-1} on average), and similar to uncertainties in the TLS-derived geodetic mass balances (± 0.13 m w.e. yr^{-1}).

1 Introduction

Around 80% of the *number* of glaciers in the European Alps (Fischer et al., 2014; Gardent et al., 2014; Fischer et al., 2015a; Smiraglia et al., 2015), and in mid- to low-latitude mountain ranges in general (Pfeffer et al., 2014), are smaller than $0.5\,\mathrm{km}^2$ and hence belong to the size class of very small glaciers according to the definition by Huss (2010). Despite their predominance in absolute number, very small glaciers have so far received little attention in glaciological research, and empirical knowledge is mainly based on studies focusing on the Mediterranean Mountains (e.g., Grunewald and Scheithauer, 2010). However, due to their vast number and short response time, very small glaciers are even relevant at larger scales, as they impact on the hydrology of certain catchments (Jost et al., 2012) and, at least over the next one or two decades, even notably contribute to global sea-level rise (Huss and Hock, 2015). Even if an increasing interest in very small glaciers of the European Alps could be observed in recent years (e.g., Hagg et al., 2008; Huss, 2010; Gilbert et al., 2012; Carturan et al., 2013; Bosson et al., 2015), field measurements are still sparse, meaning that there is considerable uncertainty in the response of very small glaciers to atmospheric warming. It is likely that currently medium-sized or even large glaciers become very small glaciers due to disintegration and substantial area loss over the next decades in areas like the European Alps (Zemp et al., 2006). A better understanding of their dynamics and sensitivity to climate change is thus important (Huss and Fischer, 2016).

Measuring glacier mass balance is important to understand the glacier-climate interaction as it directly reflects the climatic forcing on the glacier (e.g., Vincent et al., 2004). In contrast to annual field measurements on individual glaciers using the direct glaciological method (Østrem and Brugman, 1991; Cogley et al., 2011), mass balance can also be reconstructed from the comparison of two different digital elevation models (DEMs) of the glacier surface topography using the geodetic method (e.g., Rignot et al., 2003; Zemp et al., 2013). Until a few years ago, the accuracy of such DEMs, for instance derived from photogrammetry, mostly limited the time resolution of reliable geodetic mass balance measurements to a multi-annual to decadal scale (Cox and March, 2004; Thibert et al., 2008). Today, Light Detection And Ranging (LiDAR) techniques from aircraft, so-called airborne laser scanning (ALS), allows derivation of dense point clouds and hence creation of high-resolution DEMs over snow and ice and the computation of glacier surface elevation, volume and geodetic mass changes on an annual or semi-annual basis (Arnold et al., 2006; Joerg et al., 2012; Helfricht et al., 2014; Colucci et al., 2015; Piermattei et al., 2015a).

Even though the initial costs of the scanner and software license are high, terrestrial laser scanning (TLS) techniques are generally easier and more cost-efficiently applied to individual sites and on the annual to seasonal timescale compared to ALS techniques (Heritage and Large, 2009). As often nearly the entire surface of very small glaciers is visible from one single location (e.g., from a frontal moraine, an accessible mountain crest or summit, or from the opposite valley side), TLS is particularly appropriate to generate high-resolution DEMs, as well as to derive annual geodetic mass balances of very small glaciers. Thus, laborious and time-consuming in-situ measurements could be circumvented, and the spatial inter- and extrapolation of point measurements over the entire glacier surface avoided, which is known as an important source of uncertainty in direct glaciological mass balances (e.g., Zemp et al., 2013).

Since 2000, TLS has evolved into a method which is able to capture changes of the high-mountain cryosphere at very high spatio-temporal resolution (Ravanel et al., 2014). However, because the typical wavelengths emitted from former devices were absorbed by surfaces of fresh snow and bare ice, the application of TLS surveys in cryospheric sciences was first restricted to monitor the dynamics of rock walls (Rabatel et al., 2008; Abellán et al., 2009), rock glaciers (Bodin et al., 2008; Avian et al., 2009; Kummert and Delaloye, 2015), or debris-covered glaciers (Conforti et al., 2005; Avian and Bauer, 2006). A few years ago, DEM creation of snowy and icy terrain using a new generation of terrestrial LiDAR devices operating in the near infrared range became possible (Prokop et al., 2008; Schwalbe et al., 2008; Grünewald et al., 2010; Egli et al., 2012). To our knowledge, Carturan et al. (2013) were the first to compute both seasonal and annual geodetic mass balance of a very small glacier

(Montasio Occidentale, 0.07 km^2, Julian Alps, Italy) from the differencing of repeated high-resolution TLS-derived DEMs. Similar studies were to follow (e.g., López-Moreno et al., 2016, for the Monte Perdido Glacier in the Spanish Pyrenees). In the meantime, ground or Unmanned Aerial Vehicle (UAV) based close-range photogrammetry combined with computer vision algorithms such as Structure-from-Motion (SfM) has evolved into a valuable, cost-efficient and safe method to derive annual specific geodetic mass changes of small Alpine glaciers of similar quality compared to TLS or ALS techniques (Piermattei et al., 2015a, b). Although area-averaged geodetic mass balances calculated with high-resolution remote sensing survey techniques showed close agreement with glacier-wide direct glaciological balances (Piermattei et al., 2015a), validation of these emerging new methods through comparison to in-situ measurements has so far been pending. It is, however, needed to assess the quality and applicability of close-range high-resolution remote sensing techniques for glacier mass balance monitoring (Tolle et al., 2015).

In this paper we present a new data set of annual geodetic mass balances for five very small glaciers in the Swiss Alps and two consecutive years (2013/14–2014/15) calculated from the differencing of repeated TLS-derived DEMs. The LiDAR surveys were performed with a long-range terrestrial laser scanner (*Riegl* VZ-6000) enabling the acquisition of surface elevation information over snow and ice of enhanced quality and over larger areas than with previous devices working in the near infrared (Deems et al., 2015; Gabbud et al., 2015). We compare our results to direct glaciological mass balances from dense in-situ measurements and perform an in-depth uncertainty assessment of both the TLS-derived geodetic and the direct glaciological mass changes.

2   Study sites

The five study glaciers are located in the western, central, and eastern Swiss Alps (Fig. 1d). They are all smaller than 0.5 km^2, generally north-exposed, and range from 2600 to 2900 m a.s.l. for the most part (Fig. 1, Tab. 1). To better understand the response of very small glaciers in the Swiss Alps to climate change, the studied glaciers have been subject to detailed scientific research since 2006 (Pizolgletscher), 2012 (Glacier du Sex Rouge, St. Annafirn), and 2013 (Schwarzbachfirn), and a comprehensive set of empirical field data is now available for these sites.

Glacier de Prapio is a steep and crevassed cirque glacier situated below the headwalls of a rock ledge which confines a nearby and flat valley glacier (Glacier de Tsanfleuron, see e.g., Hubbard et al., 2003) to the west (Fig. 1a and 1-1). Observed area losses were smaller than for the other studied glaciers during past decades (Tab. 1).

Glacier du Sex Rouge lies west of the prominent Oldehore/Becca d'Audon (3123 m a.s.l.) (Fig. 1a and 1-2). Over
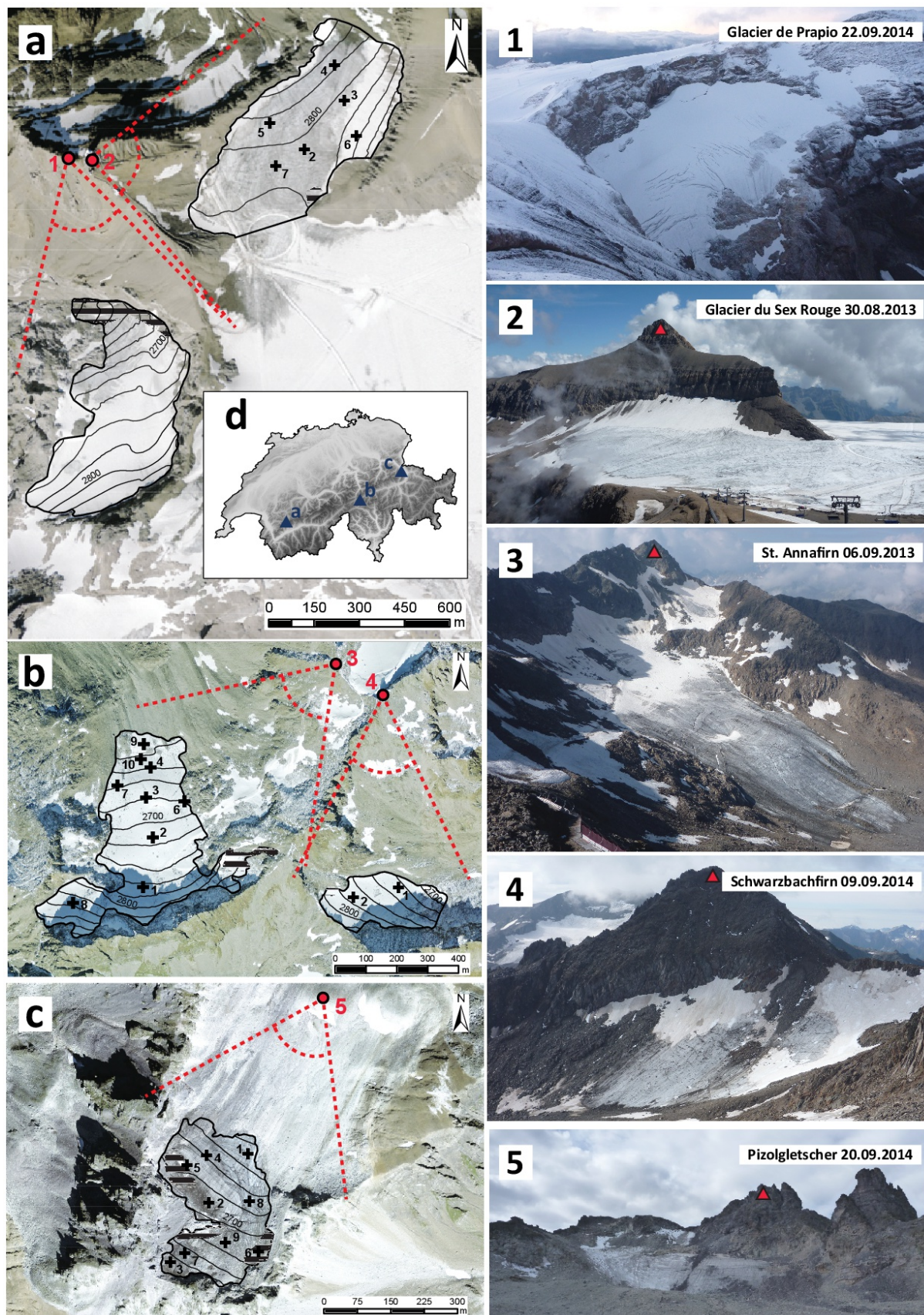
Figure 1. Overview of study sites. (a) Glacier de Prapio and Glacier du Sex Rouge, (b) St. Annafirn and Schwarzbachfirn, and (c) Pizolgletscher. The locations Terrestrial of the surveyed glaciers in the Swiss Alps is given in (d). Scan positions and horizontal view angles of the TLS surveys are shown by red dots and red dashed lines. Red numbers correspond to individual photographs of the study glaciers which were taken from the respective scan positions. Red triangles on the photographs refer to summits mentioned in the text. Black dashed areas indicate LiDAR shadow, and black crosses the locations of ablation stakes.

Table 1. Different parafs describing the characteristics of the five study sites listed from west to east: Location, surface area in 2010 (A_{2010}), relative area change between 1973 and 2010 ($\Delta A_{1973-2010}$), elevation range (Δz_{2010}) and length (L_{2010}) in 2010, and dominant aspect from the Swiss Glacier Inventory 2010 (Fischer et al., 2014). In addition, the dates of the field surveys are given.

Parameters	Glacier de Prapio	Glacier du Sex Rouge	St. Annafirn	Schwarzbachfirn	Pizolgletscher
Location	7.206°E 46.319°N	7.214°E 46.327°N	8.603°E 46.599°N	8.612°E 46.597°N	9.391°E 46.961°N
A_{2010} (km^2)	0.21	0.27	0.22	0.06	0.09
$\Delta A_{1973-2010}$ (%)	−24.6	−60.9	−50.6	−66.7	−69.7
Δz_{2010} (m a.s.l.)	2558–2854	2714–2867	2596–2928	2686–2832	2602–2783
L_{2010} (km)	0.70	0.64	0.68	0.34	0.42
Dominant aspect	NW	NW	N	NE	NE
Dates of field surveys					
autumn 2013	14.09.*	14.09.	06.09.	07.09.	23.09.
autumn 2014	22.09.*	22.09.	26.09.	26.09.	20.09.
autumn 2015	21.09.*	21.09.	28.09.	28.09.	09.09.

*only TLS surveys

a flat ice divide, the glacier is connected to Glacier de Tsanfleuron (Fig. 1a). Since 1961, the glacier lost half of its volume (Fischer et al., 2015b). Apart from pronounced area and mass loss, the glacier surface flattened over the last decades. Today, no major crevasses exist at the glacier surface, meltwater runs off in meandering supraglacial or glacier marginal channels, and downglacier horizontal surface displacement rates measured with differential Global Positioning System (dGPS) amount to 0.7 m yr^{-1}.

St. Annafirn is a cirque glacier protected by steep rock walls connecting St. Annahorn (2937 m a.s.l.) with Chastelhorn (2973 m a.s.l.) (Fig. 1b and 1-3). Kenner et al. (2011) studied the erosion of these recently deglaciated rock walls using TLS, and Haberkorn et al. (2015) their thermal regime and its relation to snow cover. By 2010, St. Annafirn shrank to half its surface area in 1973, and lost about two thirds of its volume since 1986 (Tab. 1 Fischer et al., 2015b).

Schwarzbachfirn is situated at the foot of the north face of Rothorn (2933 m a.s.l.) (Fig. 1b and 1-4). Between 1990 and 2010, the glacier lost about 85% of its total volume (Fischer et al., 2015b). Since 1973, it retreated back to one third of its initial surface area (Tab. 1).

Pizolgletscher is located below the eastern headwalls of Pizol summit (2844 m a.s.l.) and is surrounded by rock walls on three sides (Fig. 1c and 1-5). Huss (2010) pointed out the remarkable small-scale variability in accumulation and melt processes, to the importance of snow redistribution and the influence of albedo feedback mechanisms on the mass balance of this very small glacier. Pizolgletscher showed rapid retreat and lost 70% of its initial surface area between 1973 and 2010. Compared to 1961, a volume loss of 63% was observed (Tab. 1, Fischer et al. (2015b)).

3 Data and methods

3.1 TLS-derived surface elevation and mass changes

3.1.1 The *Riegl* VZ-6000 terrestrial laser scanner

TLS is an active LiDAR technique, which measures the target distance based on the time-of-flight principle, i.e. the time of an emitted laser signal required to return to its source (Deems et al., 2013). The long-range *Riegl* VZ-6000 terrestrial laser scanner was used here to produce annually repeated dense point clouds of the investigated glacier surfaces and adjacent areas, which were subsequently used to create high-resolution DEMs. Using common TLS devices with wavelengths around 1500 nm, i.e. with low reflectance but high absorption over snow and ice, the possible scanning distance is limited to a maximum of only ~150 m (Deems et al., 2013). These systems are therefore rather unsuitable for applications related to glacier monitoring. Compared to the former generation of TLS systems operating also at the lower range of the near infrared but with shorter wavelengths (so-called Class 1 laser scanners, e.g., Carturan et al., 2013), the *Riegl* VZ-6000 Class 3B laser scanning system allows faster surveys (up to 222'000 measurements s^{-1}) of larger areas and targets at greater distances (up to >6000 m) with previously unprecedented accuracy and precision. Operating at 1064 nm, the TLS system is particularly well suited for measuring snow- and ice-covered terrain (Tab. 2; RIEGL Laser Measurement Systems, 2013).

3.1.2 LiDAR surveys

Starting in September 2013, TLS surveys of the study glaciers were performed on an annual basis, coinciding with in-situ measurements on the same days to determine the direct glaciological mass balances (Tab. 1). Our approach to orient and tie subsequent scans of the same study site into

Figure 2. TLS survey of St. Annafirn in September 2014 with the *Riegl* VZ-6000 terrestrial laser scanner.

Table 2. Parameters and values of the *Riegl* VZ-6000 terrestrial laser scanner used for this study (RIEGL Laser Measurement Systems, 2013), and typical survey parameters chosen for the individual annual field surveys.

System parameters	Value (range)
Measuring range for:	
- good diffusely reflective targets	>6000 m
- bad diffusely reflective targets	>2000 m
Ranging accuracy, precision	± 15 mm, ± 10 mm
Measuring point frequency	23'000–222'000 s^{-1}
Measuring beam divergence	0.12 mrad
Laser wavelength	Near infrared (1064 nm)
Scanning range:	
- horizontal	0 to 360°
- vertical	–30 to 30°
Power supply	11-28V DC
Temperature range:	
- operational	0 to 40°C
- storage	–10 to 50°C
Weight	approx. 14.5 kg
Dimensions	236 x 226.5 x 450 mm
Chosen survey parameters	**Parameter range**
Pulse repetition frequency	30 kHz
Vertical angle increment	0.08°(2013)/0.008°(2014,2015)
Vertical angle range	60–120°from zenith
Horizontal angle increment	0.08°(2013)/0.008°(2014,2015)
Horizontal angle range	0–120°

a common coordinate system was to use the relative orientation of the scans and to define one scan as the reference to which the successive was registered (cf. section 3.1.3). Therefore, and also because nearly the entire glacier surface areas were visible from selected scan locations, it was adequate to perform the LiDAR surveys from only one single scan position for every site (in Fig. 1). Additional measurements of Ground Control Points (GCPs) with dGPS were omitted on purpose, as the potential of the long-range LiDAR system to remotely monitor surface elevation and mass changes of very small glaciers was also to be tested with the aim of reducing laborious and potentially dangerous in-situ measurements to a minimum here.

Prior to the laser scanning, the *Riegl* VZ-6000 was mounted on a tripod placed on stable surface in order to prevent ground motion and enhance data acquisition quality (Fig. 2). Because Class 3B laser scanners operate at wavelengths not inherently eye-safe, important precautions needed to be taken, including safety measures for the operators as well as people potentially moving within a predefined ocular hazard distance (RIEGL Laser Measurement Systems, 2012).

The scan parameters were chosen as a compromise between maximizing resolution (point density) over the measured area and minimizing data acquisition time (Tab. 2, Supplementary Tab. 1). In order to avoid range ambiguity and associated possible uncertainty due to several laser pulses simultaneously in the air (Rieger and Ullrich, 2012), the pulse repetition frequency was always set to 30 kHz. From the experience of the first TLS surveys in autumn 2013, it was shown to be safe enough to decrease the vertical and horizontal angle increments, i.e. increase the measurement time, by one order of magnitude. This enhanced the ground resolution of target reflections (point density) to an important extent. For all scans, average point density was 30 m^{-2} (range 1 to 95 points m^{-2}, cf. Supplementary Tab. 1). The vertical angle range was often fully utilized, while the horizontal angle range (Fig. 1a-c) had to be wider than the area of interest, i.e. the horizontal glacier extents, in order to use reflections from stable terrain outside the glaciers for the point cloud registration.

3.1.3 TLS data processing

Relative registration of the TLS point clouds was performed using RiSCAN PRO® v 2.1 (RIEGL Laser Measurement Systems, 2015). First, reflections outside the area of interest, as well as clear outliers originating from atmospheric reflections due to moisture or dust, were selected and permanently deleted. One point cloud of two consecutive scans was treated as registered. Changing surfaces (mostly reflections from snow and ice in our case) of the second, unregistered point cloud were selected and temporarily removed until it only consisted of stable terrain, i.e. preferably planar and snow- and ice-free features as rock walls or rock outcrops and large boulders outside the glacier. Manual coarse-registration was performed in order to approximatively shift the unregistered point cloud into the local coordinate system of the registered one. Therefore, a sufficient number of spatially matching points (at least four) was identified by eye on

both point clouds over stable terrain. Finally, a Multi-Station Adjustment (MSA) algorithm for semi-automatic fine registration using iterative closest point (ICP) techniques was performed (e.g., Zhang, 1992; Carrivick et al., 2013, cf. section 4.1). An octree filter (e.g., Perroy et al., 2010) was applied to the registered scans to remove noise and generate point clouds with equal numbers of reflections per area.

3.1.4 Calculation of surface elevation and geodetic mass changes

Interpolation of the processed point data sets to regular grids and calculation of surface elevation and geodetic mass changes was performed in ArcMap v 10.1. For each study site and individual time step, surface elevation changes Δh_{TLS} were calculated by differencing of the TLS-derived DEMs. No extrapolation of Δh_{TLS} was performed for areas with LiDAR shadow as it would have introduced unnecessary uncertainty. This did not hamper a direct comparison between glaciological and geodetic mass balances because the relative proportions of LiDAR shadow over the glacier surface areas were minor (0.7% for Glacier du Sex Rouge, 7.9% for Glacier de Prapio, 3.3% for St. Annafirn, 1.2% for Schwarzbachfirn, and 15.8% for Pizolgletscher, Fig. 1). Glacier volume changes ΔV (m^3) for individual sites and years were derived by multiplying the area of the TLS-derived DEM of Difference (DoD) A (m^2) with the mean surface elevation changes of all individual grid cells $\overline{\Delta h_{\text{TLS}}}$.

Three basic approaches exist to convert geodetic volume to mass changes (e.g., Huss, 2013): (1) Application of a density of volume change of 900 kg m^{-3} based on Sorge's law (Bader, 1954). This implies that neither changes in the mean firn density nor in the firn thickness and extent occur over time; (2) estimation of an average density of volume change to 850 kg m^{-3} based on typical changes in firn and ice volume over time (e.g., Zemp et al., 2013; Andreassen et al., 2016); (3) use of zonally variable conversion factors for firn and bare ice surfaces (e.g., Schiefer et al., 2007; Kääb et al., 2012). Based on information collected during field surveys (Supplementary Tab. 2) and limited ice dynamics, approach (3) was applied here. Areas of bare ice, annual or multi-annual firn were manually defined for each glacier and survey date by considering repeated aerial and oblique photographs as well as direct observations. Corresponding densities of 900 kg m^{-3} for ice ρ_{ice}, 550 kg m^{-3} for annual firn ρ_{af}, and 700 kg m^{-3} for multi-annual firn ρ_{mf} (e.g., Sold et al., 2015) were applied to calculate a glacier-wide volume-to-mass change conversion factor $f_{\Delta V}$ as

$$f_{\Delta V} = \frac{\Delta V_{\text{ice}} \cdot \rho_{\text{ice}}}{\Delta V} + \frac{\Delta V_{\text{af}} \cdot \rho_{\text{af}}}{\Delta V} + \frac{\Delta V_{\text{mf}} \cdot \rho_{\text{mf}}}{\Delta V}, \quad (1)$$

where ΔV_{ice}, ΔV_{af} and ΔV_{mf} correspond to the measured volume changes over areas of bare ice, annual or multi-

annual firn. The TLS-derived specific geodetic mass balances B_{TLS} (m w.e. yr^{-1}) were then derived by

$$B_{\text{TLS}} = \frac{\Delta V \cdot f_{\Delta V}}{A \cdot \rho_{\text{w}}}, \quad (2)$$

where ρ_{w} is the density of water. Neither firn compaction nor ice dynamics were considered to estimate the $f_{\Delta V}$ values. Due to field observations and repeated oblique and aerial orthoimagery, the spatio-temporal evolution of the firn thicknesses and extents during and prior to the measured years 2013–2015 could be assessed, and firn compaction assumed to be negligible as a result. Ice dynamics were likely negligible for the study glaciers as measured surface displacement rates (in the order of a few 10^0 m yr^{-1}) were always smaller than the resolution of the LiDAR DEMs (several 10^0 m), and dynamic thickening and thinning apparently smaller than the uncertainty in differences between TLS-derived and in-situ measured elevation changes at ablation stakes (cf. section 5.2 below).

If there was a significant amount of fresh snow at the time of the annual LiDAR surveys, additional snow depth measurements had to be carried out. Late summer snowfall events were recorded just a few days prior to the LiDAR surveys for Glacier de Prapio, Glacier du Sex Rouge (average of 0.18 m of fresh snow) and Pizolgletscher (0.20 m) in 2013 as well as for St. Annafirn and Schwarzbachfirn (both 0.30 m) in 2015. Snow probings on the glaciers with a complete spatial coverage and a median density of about 200 measurements km^{-2} were performed on the same days as the LiDAR surveys, and measured snow depth values inter- and extrapolated to the entire glacier surfaces. No snow depth measurements exist for Glacier de Prapio in 2013 due to difficult field site access. Average snow depth measured for the adjacent Glacier du Sex Rouge was therefore adopted. The final snow distribution grids were subtracted from the TLS-derived DoDs in order to calculate the actual annual volume and geodetic mass changes corrected for fresh snow.

3.2 Glaciological mass balance

3.2.1 In-situ measurements

Direct glaciological mass balance monitoring programmes including seasonal field observations started in 2006 (Pizolgletscher), 2012 (Glacier du Sex Rouge, St. Annafirn), and 2013 (Schwarzbachfirn) (Supplementary Tab. 2). Usually in April, the spatial distribution and snow-water equivalent of the end-of winter snowpack accumulated on the glacier was determined through dense manual snow probings and density measurements in snow pits (Supplementary Fig. 1, Supplementary Tab. 2). To quantify the amount of estival mass loss through snow and ice melt and to determine the annual mass balance, 4 m ablation stakes were drilled into the glaciers with a steam drill (Fig. 1), and read out at the end of the melting season (September). Where mass gain through firn and

snow accumulation occurred, respective heights were converted into mass applying typical values for snow and firn densities from the literature.

3.2.2 Derivation of the spatial mass balance distribution from in-situ measurements

An accumulation and distributed temperature-index melt model (Hock, 1999) was applied to derive the spatial surface mass balance distribution of the four glaciers with direct measurements in daily resolution. Using a semi-automated procedure, the model was calibrated for each glacier and year individually to optimally match all seasonal field data. Taking into account the principal factors governing the accumulation and melt processes, the model can thus be regarded as a statistical tool for the spatio-temporal inter- and extrapolation of seasonal point mass balance measurements. In addition to the field measurements, required model inputs included updated glacier extents and DEMs of the glacier surfaces, as well as daily air temperature and precipitation data from nearby MeteoSwiss weather stations. A detailed description of the methodology to infer distributed mass balance is given in Huss et al. (2009) or Sold et al. (2016).

4 Uncertainty assessment

4.1 TLS-derived geodetic mass changes

Uncertainty in the TLS-derived surface elevation changes presented here can be attributed to two main sources: (1) LiDAR data acquisition errors, and (2) data processing errors and DEM creation. In the following, important aspects of these errors relevant to our methodological approach are assessed first. Then, we describe how we quantify the effective uncertainty in the TLS-derived surface elevation and geodetic mass changes.

Provided that the *Riegl* VZ-6000 used here operated reliably and ground motion was prohibited while scanning, errors in the acquired LiDAR point clouds of the surveyed glacier surfaces and surrounding areas are either terrain-induced or originate from the TLS system itself. Even though they vary in reality, for instance with the distance to the target, manufacturers commonly provide simplified and constant values for the ranging accuracy and precision of their TLS systems. For the purpose of this study, the respective values given in Table 2 for the *Riegl* VZ-6000 are assumed to apply. Terrain-induced or geometric errors arise from the surface characteristics and orientation of the target relative to the scanner, i.e. slope and aspect, and from the laser-beam divergence, i.e. size of the laser-beam footprint at the target (Schürch et al., 2011; Deems et al., 2013; Hartzell et al., 2015).

Fine registration of two consecutive point clouds is an important LiDAR post-processing step and primarily enhances the quality of TLS-derived surface elevation changes (Prokop
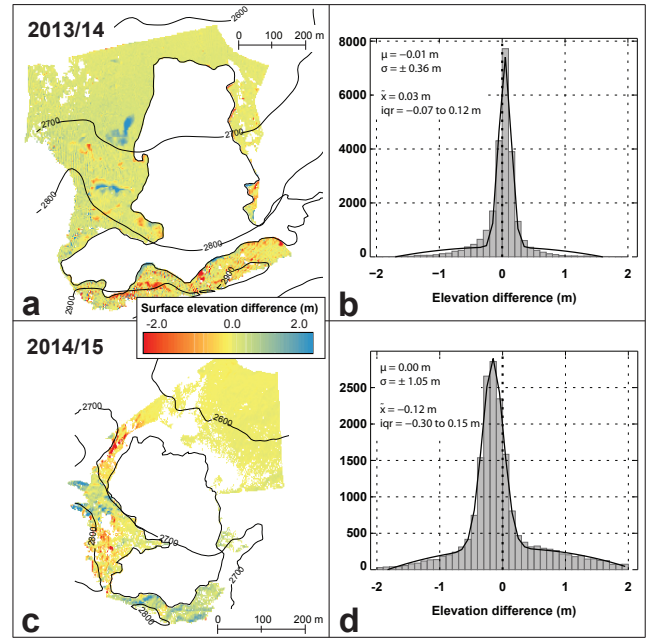
Figure 3. Comparison of annual surface elevation changes over stable terrain obtained by differencing of TLS-derived DEMs from two consecutive years. Spatial and corresponding frequency distributions of these changes for (a,b) St. Annafirn (2013/14) and (c,d) Pizolgletscher (2014/15). The black curves in (b) and (d) are normal fits over the data. In addition, the mean (μ) and median ($\tilde{x}$) elevation differences, as well as corresponding standard deviations (σ) and interquartile ranges (iqr) are given.

and Panholzer, 2009). For our study, fine registration using MSA/ICP algorithms is indispensable as no absolute registration via GCPs is performed but only selected areas of the point clouds over stable terrain are used for the relative orientation of the scans. RiSCAN PRO® delivers error statistics of the final MSA results, including a full set of fitted point residuals. The standard deviation of errors from the point residuals (σ_{MSA}) can be used to quantify the quality of the registration process and to define limits of detection for the TLS-derived surface elevation changes (Gabbud et al., 2015). σ_{MSA} ranged from ± 0.05 to ± 0.18 m (± 0.12 m on average) over stable terrain surrounding the five glaciers in individual years (Tab. 3). Reliable results require use of some 10^4 points for the MSA/ICP fine registration techniques applied here, the mean error to be zero and random errors to be Gaussian and pairwise uncorrelated (*Riegl*, personal communication, 2013). The latter two conditions are always fulfilled, whereas, due to the lower resolution (lower point densities) of the 2013 scans (Supplementary Tab. 1) and hence the lower number of points n used for the fine registration of consecutive point clouds (Tab. 3), MSA results and accordingly also registration quality have to be handled with some reservation for the observation period 2013/14.

Table 3. Limits of detection for the TLS-derived surface elevation changes (σ_{MSA}) and number of points used for the Multi-Station Adjustment fine registration of consecutive point clouds (n) for both observation periods and the surveyed Glacier de Prapio, Glacier du Sex Rouge, St. Annafirn, Schwarzbachfirn, and Pizolgletscher. In addition, the mean (μ), median ($\tilde{x}$), standard deviation (σ) and interquartile range (iqr) of elevation differences from the comparison of TLS-derived annual surface elevation changes over stable terrain (all in m) are given.

hydrological year	σ_{MSA}	n	μ	$\tilde{x}$	σ	iqr
Glacier de Prapio						
2013/14	0.07	2940	–0.18	–0.20	0.49	–0.74 to –0.07
2014/15	0.14	62902	–0.05	–0.03	1.11	–0.79 to 0.72
Glacier du Sex Rouge						
2013/14	0.18	1628	–0.02	–0.12	0.35	–0.39 to 0.34
2014/15	0.05	48270	–0.04	–0.05	0.62	–0.51 to 0.48
St. Annafirn						
2013/14	0.07	2486	–0.01	0.03	0.36	–0.07 to 0.12
2014/15	0.09	20896	0.17	0.18	0.59	–0.08 to 0.42
Schwarzbachfirn						
2013/14	0.17	7320	–0.01	–0.01	0.37	–0.17 to 0.19
2014/15	0.08	11567	0.22	0.20	0.34	0.01 to 0.24
Pizolgletscher						
2013/14	0.07	1931	0.01	–0.04	0.73	–0.21 to 0.11
2014/15	0.14	10766	0.00	–0.12	1.05	–0.30 to 0.15

Finally, point cloud filtering and gridding for DEM creation induces smoothing of the terrain information and additional error (Prokop and Panholzer, 2009; Deems et al., 2015). The quality of the TLS-derived DEMs is dependent on the LiDAR data acquisition and processing and the respective errors mentioned above. It increases with higher densities of points reflected from the surveyed terrain, which in turn depends on the chosen survey parameters (Tab. 2), surface characteristics, type and flatness of the terrain (Carrivick et al., 2013).

The accuracy of the TLS-derived surface elevation changes and possible trends in elevation differences are assessed by comparison of consecutive DEMs over stable terrain outside the glaciers (examples for St. Annafirn in 2013/14 and Pizolgletscher in 2014/15 in Fig. 3). Except for Glacier de Prapio in 2013/14 (probably due to poor registration) as well as St. Annafirn and Schwarzbachfirn in 2014/15 (due to significant amounts of fresh snow in autumn 2015), the deviations from zero regarding the mean (μ) and median ($\tilde{x}$) offsets over stable terrain between consecutive DEMs are always smaller than the limits of detection (σ_{MSA}) (Tab. 3, Fig. 3b,d). A significant trend towards higher biases in DEM differencing with steeper slopes is found (linear correlation coefficient $r = 0.96$). Remarkable elevation differences over comparably gently-sloping terrain can be attributed to changing surfaces such as snow patches (e.g., left of St. Annafirn, cf. Fig. 2 vs. 3a). For the steep rock walls confining St. Annafirn to the south, mean 2013/14 elevation differences are –0.23 m (standard deviation ±0.63 m) (Fig. 3a). This corresponds to 3.5 times the mean annual erosion rates measured by Kenner et al. (2011) and hence points to the limitations of TLS-derived elevation differences over very steep terrain (>50°) using our approach. Elevation differences outside Pizolgletscher for the period 2014/15 are also largest for the steep rock walls surrounding the glacier (Fig. 3c). Furthermore, probably some systematic error in one of the TLS-derived DEMs of Pizolgletscher results in a slight surface tilt (e.g., Lane et al., 2004) in lower left to upper right direction, which we, however, do not correct for.

The uncertainty in the average TLS-derived surface elevation changes ($\sigma_{\overline{\Delta h_{\mathrm{TLS}}}}$) for individual glaciers and years is assessed according to a simple implementation of Rolstad et al. (2009), and calculated with

$$\sigma_{\overline{\Delta h_{\mathrm{TLS}}}} = \pm \sqrt{\sigma_{\Delta h_{\mathrm{TLS}}}^2 \cdot \frac{A_{\mathrm{cor}}}{5 \cdot A}}, \qquad (3)$$

where A_{cor} is the range over which errors in DEM differencing are spatially correlated, conservatively estimated by $A_{\mathrm{cor}} = A$. $\sigma_{\Delta h_{\mathrm{TLS}}}$ is the standard deviation of errors in TLS-derived glacier surface elevation changes, area-weighted for classes of equal surface slope, for which values are derived by taking the standard deviation of elevation differences per slope class from individual DoDs over stable terrain. Values for $\sigma_{\Delta h_{\mathrm{TLS}}}$ range from ±0.26 m for the flatter glaciers like Glacier du Sex Rouge to ±0.35 m for steeper glaciers like Glacier de Prapio.

The uncertainties in the densities for ice $\sigma_{\rho_{\mathrm{ice}}}$ (estimated as ±20 kg m^{-3} here), annual and multi-annual firn $\sigma_{\rho_{\mathrm{af}}}$ and $\sigma_{\rho_{\mathrm{mf}}}$ (both assumed as ±100 kg m^{-3}) are used to estimate

the uncertainty in the glacier-wide conversion factor $\sigma_{f_{\Delta V}}$ by

$$\sigma_{f_{\Delta V}} = \frac{\Delta V_{\mathrm{ice}} \cdot \sigma_{\rho_{\mathrm{ice}}}}{\Delta V} + \frac{\Delta V_{\mathrm{af}} \cdot \sigma_{\rho_{\mathrm{af}}}}{\Delta V} + \frac{\Delta V_{\mathrm{mf}} \cdot \sigma_{\rho_{\mathrm{mf}}}}{\Delta V}. \quad (4)$$

Finally, the uncertainty in the TLS-derived annual geodetic mass balance $\sigma_{B_{\mathrm{TLS}}}$ (m w.e.) is calculated following Huss et al. (2009) as

$$\sigma_{B_{\mathrm{TLS}}} = \pm \sqrt{(\overline{\Delta h_{\mathrm{TLS}}} \cdot \sigma_{f_{\Delta V}})^2 + (f_{\Delta V} \cdot \sigma_{\overline{\Delta h_{\mathrm{TLS}}}})^2 + \sigma_{\mathrm{s}}^2}, \quad (5)$$

where $\overline{\Delta h_{\mathrm{TLS}}}$ is the glacier-wide mean of TLS-derived surface elevation changes, and σ_{s} the uncertainty in correcting measured surface elevation changes for fresh snow, which is estimated by $\pm 20\%$ of the average measured snow depth. Resulting values for $\sigma_{B_{\mathrm{TLS}}}$ are listed in Table 4 and discussed in section 6.

4.2 Direct glaciological method

Uncertainty in both point and glacier-specific annual mass balance from direct field observations has often been estimated as ± 0.2 m w.e. yr^{-1} (e.g., Dyurgerov, 2002). In-depth assessments of random and systematic errors in glaciological mass balances of selected measured glaciers showed, however, that the actual uncertainty can significantly deviate from such static estimates (Thibert et al., 2008; Zemp et al., 2013; Beedle et al., 2014).

Uncertainty in the direct glaciological method either originates from measurement errors at individual point locations, from the representativeness of the measurement sites for their close surroundings, from the spatial inter- and extrapolation and averaging of these results over the whole glacier, or from changes in the glacier geometry (Zemp et al., 2013). The latter is assumed to be negligible here as annually updated glacier outlines derived from high-resolution aerial imagery and in-situ GPS measurements are used. All stakes were located in the ablation areas of the glaciers in autumn 2014 and 2015. The uncertainty in the direct glaciological mass balance arising from measurement errors at individual stakes σ_{abl} (m w.e. yr^{-1}) is estimated following Thibert et al. (2008) by $\sigma_{\mathrm{abl}} = 0.14 / \sqrt{N_{\mathrm{abl}}}$, where N_{abl} is the number of ablation measurements for individual glaciers and years. Uncertainty from the spatial inter- and extrapolation of point measurements $\sigma_{\mathrm{int/ext}}$ (m w.e. yr^{-1}) can arise from a non-representative spatial distribution and/or insufficient density of stakes over the glacier, but is also related to the method chosen for extrapolating the mass balance to the entire glacier. $\sigma_{\mathrm{int/ext}}$ is assessed by rerunning the mass balance model by Huss et al. (2009) used for calculating glacier-wide mass balance (cf. section 3.2.2) by closely constraining it with the seasonal field data for each site and observation period but melt parameters and temperature lapse rates that
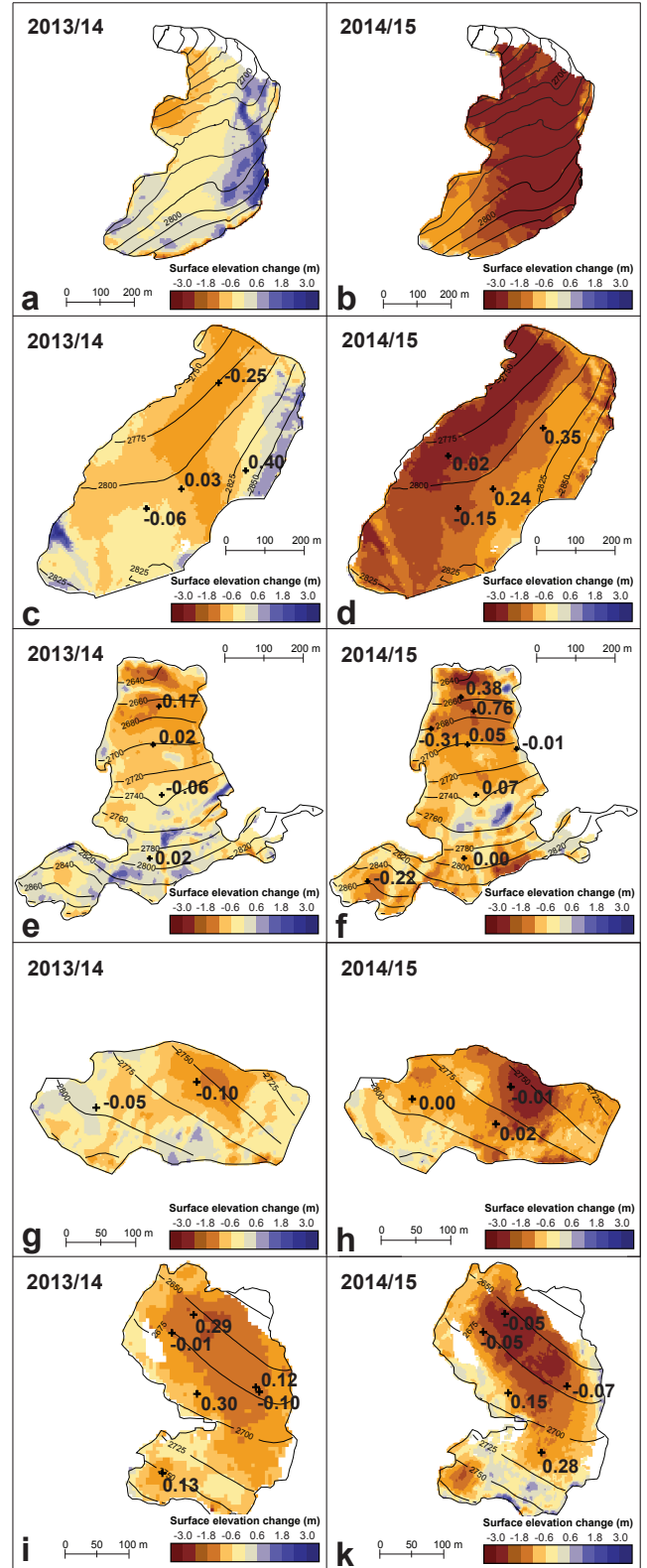
Figure 4. Spatial distribution of TLS-derived annual surface elevation changes Δh_{TLS} for (a,b) Glacier de Prapio, (c,d) Glacier du Sex Rouge, (e,f) St. Annafirn, (g,h) Schwarzbachfirn, and (i,k) Pizolgletscher in 2013/14 and 2014/15. The numbers indicate the differences (in m) between TLS-derived and in-situ measured annual elevation changes at ablation stakes (Δh_{TLS} minus $\Delta h_{\mathrm{direct}}$). White areas correspond to LiDAR shadow.
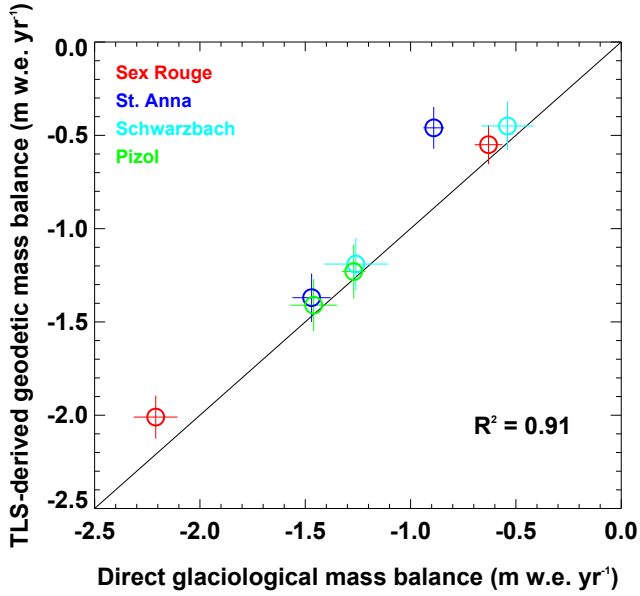
Figure 5. Direct glaciological vs. TLS-derived glacier-wide mass balances for Glacier du Sex Rouge, St. Annafirn, Schwarzbachfirn, and Pizolgletscher for the years 2013/14–2014/15. Error bars indicate the uncertainty ranges of both methods.

Table 4. Glacier-wide mean of TLS-derived surface elevation changes ($\overline{\Delta h_{\mathrm{TLS}}}$) (in m) as well as specific geodetic (B_{TLS}) and direct glaciological (B_{direct}) annual mass balance variables with corresponding uncertainties (in m w.e.) for Glacier de Prapio, Glacier du Sex Rouge, St. Annafirn, Schwarzbachfirn, and Pizolgletscher, and the two observation periods 2013/14 and 2014/15.

hydrological year	$\overline{\Delta h_{\mathrm{TLS}}}$	B_{TLS}	B_{direct}
Glacier de Prapio			
2013/14	–0.01	0.02 ±0.53	——
2014/15	–3.19	–2.58 ±0.15	——
Glacier du Sex Rouge			
2013/14	–0.66	–0.55 ±0.10	–0.63 ±0.07
2014/15	–2.41	–2.01 ±0.12	–2.21 ±0.10
St. Annafirn			
2013/14	–0.49	–0.46 ±0.11	–0.89 ±0.05
2014/15	–1.07	–1.37 ±0.13	–1.47 ±0.09
Schwarzbachfirn			
2013/14	–0.55	–0.45 ±0.13	–0.54 ±0.12
2014/15	–1.13	–1.19 ±0.14	–1.26 ±0.15
Pizolgletscher			
2013/14	–1.40	–1.23 ±0.15	–1.27 ±0.06
2014/15	–1.40	–1.41 ±0.14	–1.46 ±0.11

differed from the reference values by predefined ranges (cf. Kronenberg et al., 2016). In our approach, also the uncertainty in the measured winter snow accumulation distribution influences the spatial patterns of evaluated annual direct glaciological mass balance. It originates from both snow accumulation measurement errors σ_{acc} (m w.e. yr^{-1}) and errors in measured density of the winter snowpack $\sigma_{\rho_{\mathrm{s}}}$ (m w.e. yr^{-1}). The former is estimated by $\sigma_{\mathrm{acc}} = 0.21/\sqrt{N_{\mathrm{acc}}}$ (Thibert et al., 2008), where N_{acc} is the number of winter snow depth measurements for individual glaciers and years, the latter by rerunning the mass balance model with values for $\sigma_{\rho_{\mathrm{s}}}$ that differ by ±10% from the measured ones. Finally, the uncertainty in the annual direct glaciological mass balance $\sigma_{B_{\mathrm{direct}}}$ (m w.e.) is calculated with

$$\sigma_{B_{\mathrm{direct}}} = \pm\sqrt{\sigma_{\mathrm{abl}}^2 + \sigma_{\mathrm{int/ext}}^2 + \sigma_{\mathrm{acc}}^2 + \sigma_{\rho_{\mathrm{s}}}^2}. \qquad (6)$$

Resulting values for $\sigma_{B_{\mathrm{direct}}}$ are listed in Table 4 and discussed in section 6.

5 Results

5.1 TLS-derived surface elevation and geodetic mass changes

Except for Glacier de Prapio in 2013/14 with balanced average conditions, all of the investigated glaciers showed clearly negative surface elevation and geodetic mass changes for the

hydrological years 2013/14–2014/15 (Fig. 4, Tab. 4). Measured mass losses were remarkably stronger for the second time period (–1.65 m w.e. in 2014/15 averaged for the four glaciers measured with both methods compared to –0.59 m w.e. in 2013/14), which agrees well with the different prevailing atmospheric conditions (especially in summer) recorded during the observed years (MeteoSwiss, 2015, 2016). Moreover, clear differences in glacier changes could be observed for individual sites in both years. In 2013/14, resulting surface elevation and mass changes of Pizolgletscher situated in the eastern Swiss Alps were significantly more negative compared to St. Annafirn and Schwarzbachfirn in the central Swiss Alps and Glacier de Prapio and Glacier du Sex Rouge in the western Swiss Alps. In 2014/15, though, the glaciers of the western Swiss Alps showed by far the strongest mass losses. Measured changes were also more negative for glaciers of the central Swiss Alps, but only slightly more negative for Pizolgletscher compared to the precedent year. These regional differences in observed mass balances are consistent with those reported for all monitored glaciers in Switzerland in 2013/14 and 2014/15 (Huss et al., 2015). The very small glaciers investigated here thus showed a similar response to the observed climatic forcing compared to larger glaciers, demonstrating that they are valuable indicators of mass balance variability despite their limited size.

A remarkably high small-scale variability in the spatial distribution of TLS-derived annual surface elevation changes is unveiled in Figure 4. Independent of the glacier-wide
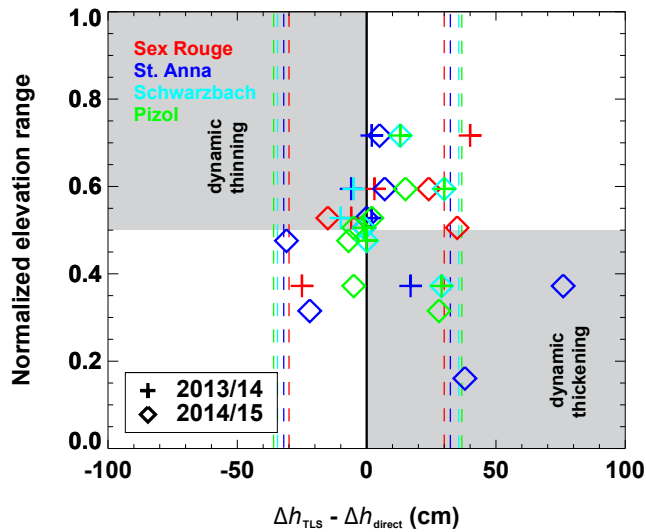
Figure 6. Differences between TLS-derived (Δh_{TLS}) and observed ($\Delta h_{\mathrm{direct}}$) annual surface elevation changes at ablation stakes vs. normalized elevation range for Glacier du Sex Rouge, St. Annafirn, Schwarzbachfirn, and Pizolgletscher for 2013/14 and 2014/15. Dashed vertical lines indicate the uncertainty ranges of Δh_{TLS} minus $\Delta h_{\mathrm{direct}}$ relative to zero. Grey quadrants mark the theoretical ranges of Δh_{TLS} minus $\Delta h_{\mathrm{direct}}$ vs. normalized elevation range for glaciers in equilibrium.

mean values varying for individual sites and years (Tab. 4), the variance in the TLS-derived surface elevation changes expressed by its 1σ standard deviation was similar for all glaciers (± 0.81 m on average evaluated over the elevation ranges of about 100–300 m for individual glaciers). Moreover, a two-sample t-test showed that the magnitude of the spatial variability in Δh_{TLS} did not significantly change between 2013/14 and 2014/15, either.

5.2 Comparison to direct glaciological mass balances

The TLS-derived geodetic mass balances showed a close match with the direct glaciological mass balances extrapolated from in-situ measurements. Observed geodetic mass changes were slightly but systematically less negative compared to direct glaciological ones (Fig. 5, Tab. 4). Applying the statistical tests and approach proposed by Zemp et al. (2013), we validated the geodetic against the direct glaciological mass balances, and found that the differences in the resulting values between both methods were, except for St. Annafirn in 2013/14, not significant (95% confidence level). Corresponding uncertainties in the annual mass balances did, according to the results of a two-sample t-test, not differ significantly between both methods, either.

The most prominent patterns in the observed spatial distribution of annual direct glaciological mass balances were

captured by the TLS-derived surface elevation changes (Supplementary Fig. 1 vs. Fig. 4). The high-resolution LiDAR DEMs, however, allowed uncovering a level of detail in annual surface elevation changes unequalled by the direct mass balance observations.

In order to directly compare the extrapolated local mass balances from in-situ measurements to TLS-derived elevation changes, we multiplied the distributed direct glaciological mass balances with the reciprocal values of respective zonal conversion factors. Self-evidently, such confrontations of TLS-derived surface elevation changes to surface mass balances are only valid under the assumption that internal and basal mass balance components as well as dynamic thickening and thinning are negligible or absent. For larger glaciers, this is clearly not true (Fischer, 2011; Sold et al., 2013; Beedle et al., 2014). The comparison of differences between TLS-derived (Δh_{TLS}) and in-situ measured ($\Delta h_{\mathrm{direct}}$) annual surface elevation changes at individual ablation stakes of Glacier du Sex Rouge, St. Annafirn, Schwarzbachfirn, and Pizolgletscher indicated, however, that dynamic thickening and thinning was minor and negligible for the very small glaciers studied here. The differences in surface elevation changes were close to zero for the majority of the point measurements (Fig. 6). Furthermore, the uncertainties in Δh_{TLS} minus $\Delta h_{\mathrm{direct}}$ calculated as $\pm\sqrt{\sigma_{\Delta h_{\mathrm{TLS}}}^2 + \sigma_{\mathrm{abl}}^2}$ were mostly greater than the measured differences themselves (Fig. 6), which would hamper inferring dynamic thickening and thinning from these data. We therefore argue that applying reciprocal zonal conversion factors to the surface mass changes and hence also the spatial patterns of differences in Δh_{TLS} and $\Delta h_{\mathrm{direct}}$ (Fig. 7) are presumably robust enough for qualitative but direct comparisons of both methods with respect to very small glaciers.

For Glacier du Sex Rouge and Pizolgletscher, mean (μ) and median ($\tilde{x}$) differences between $\Delta h_{\mathrm{direct}}$ and Δh_{TLS} were slightly negative on average, indicating that direct glaciological elevation changes were more negative than those based on the LiDAR DEMs (Fig. 7b,e). Over most of the glacier surface, both methods showed very similar results. On the other hand, remarkable differences in surface elevation changes were found for distinct, mostly steeper and/or glacier-marginal areas (Fig. 7a,c,d,f). For Glacier du Sex Rouge in 2014/15, such disagreements were quite restricted to areas with no in-situ measurements. Furthermore, surface elevation changes over areas influenced by anthropogenic activity like a glacier walk maintained by snowcats (Fig. 7a) showed clear differences between Δh_{TLS} and $\Delta h_{\mathrm{direct}}$.

6 Applicability of the TLS system for mass balance monitoring of very small Alpine glaciers

On average, the uncertainty in the TLS-derived annual specific geodetic mass balances $\sigma_{B_{\mathrm{TLS}}}$ of the four very small
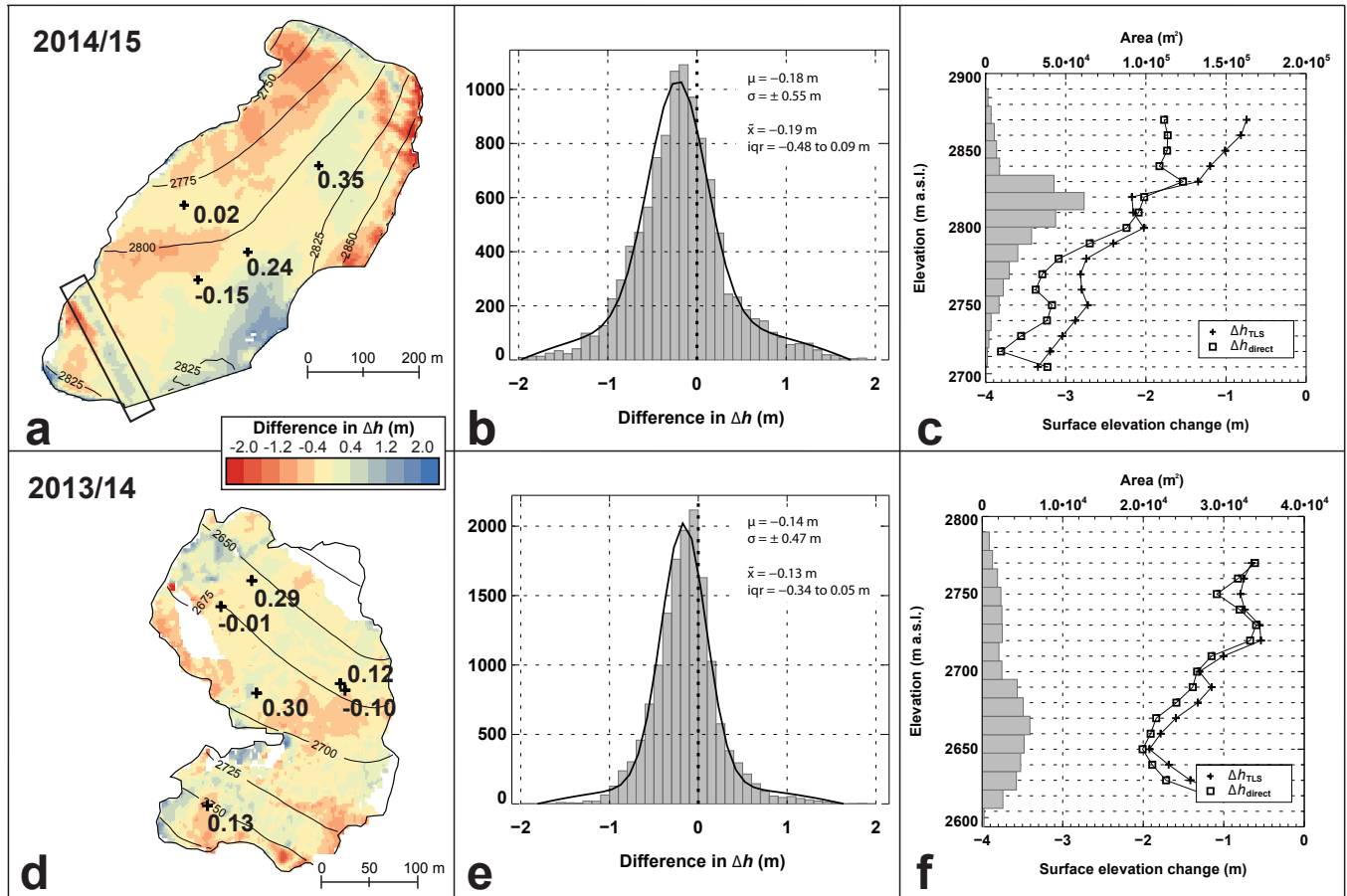
Figure 7. Difference between TLS-derived surface elevation changes and extrapolated glaciological mass balances which were converted to surface elevation changes by multiplication with the respective reciprocal values of zonal conversion factors. Spatial and corresponding frequency distributions as well as distributions of these changes vs. surface hypsometry for (a,b,c) Glacier du Sex Rouge (2014/15) and (d,e,f) Pizolgletscher (2013/14). The numbers in (a) and (d) indicate the differences (in m) between TLS-derived and in-situ measured annual elevation changes at ablation stakes (Δh_{TLS} minus $\Delta h_{\mathrm{direct}}$). The rectangle in (a) highlights a linear feature originating from a glacier walk maintained by snowcats. The black curves in (b) and (e) are normal fits over the data. In addition, the mean (μ) and median ($\tilde{x}$) elevation differences, as well as corresponding standard deviations (σ) and interquartile ranges (iqr) are given.

glaciers in Switzerland measured with both methods is ± 0.13 m w.e. yr^{-1} (Tab. 4). The accuracy of our results is thus similar to geodetic mass changes computed over pentadal to decadal time periods based on high-resolution source data (e.g., Andreassen et al., 2016; Magnússon et al., 2016). Even though we consider our approach to quantify both $\sigma_{B_{\mathrm{TLS}}}$ and $\sigma_{B_{\mathrm{direct}}}$ as robust and promote its application to similar studies in the future, we want to remind the reader that it is generally difficult to give exact numbers of such uncertainties, and that each component of $\sigma_{B_{\mathrm{TLS}}}$ and $\sigma_{B_{\mathrm{direct}}}$ is based on assumptions that are, to some extent, uncertain themselves. By its nature, the stochastic uncertainty in the glacier-wide TLS-derived geodetic mass balance $\sigma_{B_{\mathrm{TLS}}}$ is much lower than the potential error in the observed surface elevation changes for single pixels, as estimated for instance from the comparison of DoDs over stable terrain (Fig. 3).

Uncertainty in the glacier-wide annual direct glaciological mass balances $\sigma_{B_{\mathrm{direct}}}$ of Glacier du Sex Rouge, St. Annafirn, Schwarzbachfirn and Pizolgletscher is ± 0.09 m w.e. yr^{-1} on average (Tab. 4), and hence comparable to the mean $\sigma_{B_{\mathrm{TLS}}}$. Resulting values for $\sigma_{B_{\mathrm{direct}}}$ presented here are similar to those reported for Storglaciären (Jansson, 1999), but significantly smaller compared to the majority of all measured glaciers worldwide (e.g., Thibert et al., 2008; Beedle et al., 2014; Andreassen et al., 2016). This can be attributed to the higher density and more complete coverage of winter and summer point measurements for our study glaciers than for most other glaciers (Supplementary Tab. 2; WGMS, 2013). Their very small surface area and the absence or minor fractions of very steep and/or heavily crevassed zones are, of course, optimal preconditions to accurately measure direct glaciological mass balance.

Hence, the quality of both the geodetic mass balances derived by repeated terrestrial LiDAR surveys and the direct glaciological mass balances extrapolated from dense in-situ measurements is very good. As resulting values of B_{TLS} for individual glaciers and years do not significantly differ from the respective values of B_{direct}, we recommend the application of terrestrial laser scanning for future mass balance monitoring of very small Alpine glaciers. From our experience, however, a number of prerequisites needs to be fulfilled in order to obtain reliable results, including (1) the absence of significant amounts of firn or fresh snow at the moment of the LiDAR survey at the end of the melting season; (2) the abundance and visibility of sufficient areas of stable terrain surrounding the entire glacier in order to achieve a good quality of the relative registration of consecutive LiDAR scans; and (3) good weather conditions (dry atmosphere). Frontal scan settings further increase the data quality.

Significant amounts of fresh snow or firn on the glacier results in more error-prone conversions of TLS-derived volume to mass changes, even more if no additional in-situ measurements of their area fraction and density are performed. On the other hand, from field evidence we know that along with the recorded atmospheric conditions (especially in summer) and the continuously negative mass balance context in the Swiss Alps over the last decade (WGMS, 2012; Huss et al., 2015), the studied very small glaciers hardly exhibit significant ratios of annual to perennial snow and firn anymore. This is of course in favour of reliable TLS-based geodetic mass balance monitoring. Considerable firn extents and volumes can, however, rebuild on very small glaciers within a short time (e.g., over only one year) (Kuhn, 1995), which would again induce higher uncertainty in B_{TLS}.

Disadvantages of using the long-range TLS system and our approach to derive annual surface elevation and geodetic mass changes of very small Alpine glaciers are the high costs for the purchase of the device itself and licenses for the data analysis software provided by the manufacturer, as well as the complex and time-consuming post-processing of the LiDAR data. The required level of expertise and experience with TLS data acquisition and processing is likely higher than for direct glaciological mass balance monitoring (see e.g., Ravanel et al., 2014). In addition, the possibility to ensure safety, i. e. guarantee that no person other than the instrument operators wearing protection glasses moves within a predefined ocular hazard distance, often proves to be non-trivial, especially in well-developed areas like the Alps.

7   Conclusions

Despite their global predominance in absolute number, empirical field data on very small glaciers, here defined as being smaller than $0.5\,\text{km}^2$, are currently sparse. In consequence, our understanding of their response to changes in the climatic forcing is still unsatisfactory. Monitoring surface elevation and mass changes of very small glaciers at high spatio-temporal resolution is a prerequisite to solve this problem. Terrestrial laser scanning has evolved into a method which is able to fulfil these requirements. Because often almost the entire surface of very small glaciers is visible from one single location, it is a highly promising technique to create repeated high-resolution DEMs and subsequently compute geodetic surface elevation and mass changes of the smallest glaciers.

Here, we presented the application of a long-range terrestrial laser scanner (*Riegl* VZ-6000) especially designed for surveying snow- and ice-covered terrain. We derived annual surface elevation and geodetic mass changes of five very small glaciers in Switzerland (Glacier de Prapio, Glacier du Sex Rouge, St. Annafirn, Schwarzbachfirn, and Pizolgletscher) over two consecutive years (2013/14–2014/15). Because validation of geodetic mass changes derived from repeated TLS surveys or other emerging close-range high-resolution remote sensing techniques is still pending, we compared our results to direct glaciological mass balances from dense in-situ measurements coinciding with the LiDAR surveys and performed an in-depth accuracy assessment of both methods.

Resulting surface elevation and geodetic mass changes were generally negative, showing different regional mass balance patterns but stable and high small-scale variability in both years. Remarkably stronger mass losses were measured for the second time period (–1.65 m w.e. in 2014/15 averaged for the four glaciers measured with both methods compared to –0.59 m w.e. in 2013/14). TLS-derived specific geodetic mass balances were slightly less negative but did not vary significantly compared to direct glaciological mass balances extrapolated from in-situ measurements ($R^2 = 0.91$).

Uncertainty in the TLS-derived surface elevation changes can be attributed to LiDAR data acquisition errors, data processing errors and DEM creation. For geodetic mass changes, additional uncertainty results from the conversion of volume to mass changes. Mean uncertainty in the TLS-derived annual specific geodetic mass balances $\sigma_{B_{\text{TLS}}}$ was $\pm 0.13\,\text{m}$ w.e. Uncertainty in the direct glaciological annual mass balances was similar ($\pm 0.09\,\text{m}$ w.e. on average) and, due to the dense in-situ measurements, rather small compared to the majority of measured glaciers worldwide.

Our results show that, under some restrictions, the TLS-based monitoring approach presented in this paper yields accurate results and is therefore suitable for repeated mass balance measurements of very small Alpine glaciers. The most important shortcomings of our approach are related to the abundance of snow and firn at the time of the TLS surveys. They are insignificant in a highly negative mass balance context, as observed for instance for most of our field sites over the last years. Under these circumstances, laborious, time-consuming, and potentially dangerous field measurements may be circumvented and the uncertain spatial inter- and extrapolation of point measurements over the whole glacier surface avoided.

Acknowledgements. This study is supported by the Swiss National Science Foundation (SNSF), grant 200021_137586. Sincere and many thanks to numerous friends and colleagues for their assistance in the field, and to Gstaad 3000 AG (K. von Siebenthal), Andermatt Gotthard Sportbahnen AG (C. Danioth), and Pizolbahnen AG for technical support and free transportation. Furthermore, we want to thank C. Gabbud, S. Gindraux, J.-B. Bosson and J. Carrivick for their earlier comments on this manuscript. Finally, thanks to the scientific editor A. Vieli, J. I. López-Moreno and two anonymous reviewers for their work, which helped finalizing the paper.

References

Abellán, A., Jaboyedoff, M., Oppikofer, T., and Vilaplana, J. M.: Detection of millimetric deformation using a terrestrial laser scanner: experiment and application to a rockfall event, Nat. Hazards Earth Syst. Sci., 9, 365–372, doi:10.5194/nhess-9-365-2009, 2009.

Andreassen, L. M., Elvehøy, H., Kjøllmoen, B., and Engeset, R. V.: Reanalysis of long-term series of glaciological and geodetic mass balance for 10 Norwegian glaciers, The Cryosphere, 10, 535–552, doi:10.5194/tc-10-535-2016, 2016.

Arnold, N. S., Rees, W. G., Devereux, B. J., and Amable, G. S.: Evaluating the potential of high-resolution airborne LiDAR data in glaciology, Int. J. Remote Sens., 27(6), 1233–1251, doi:10.1080/01431160500353817, 2006.

Avian, M. and Bauer, A.: First Results on Monitoring Glacier Dynamics with the Aid of Terrestrial Laser Scanning on Pasterze Glacier (Hohe Tauern, Austria), 8th International Symposium on High Mountain Remote Sensing Cartography, La Paz, Bolivia, 27–35, 2006.

Avian, M., Kellerer-Pirklbauer, A., and Bauer, A.: LiDAR for monitoring mass movements in permafrost environments at the cirque Hinteres Langtal, Austria, between 2000 and 2008, Nat. Hazards Earth Syst. Sci., 9, 1087–1094, doi:10.5194/nhess-9-1087-2009, 2009.

Bodin, X., Schoeneich, P., and Jaillet, S.: High-resolution DEM extraction from terrestrial LIDAR topometry and surface kinematics of the creeping alpine permafrost: The Laurichard rock glacier case study (Southern French Alps), edited by: Kane, D. L. and Hinkel, K. M.: Ninth International Conference on Permafrost. Institute of Northern Engineering, University of Alaska at Fairbanks, 1, 137–142, 2008.

Bader, H.: Sorge's law of densification of snow on high polar glaciers, J. Glaciol., 2(15), 319–323, 1954.

Beedle, M. J., Menounos, B., and Wheate, R.: An evaluation of mass-balance methods applied to Castle Creek Glacier, British Columbia, Canada, J. Glaciol., 60(220), 262–276, doi:10.3189/2014JoG13J091, 2014.

Bosson, J.-B., Deline, P., Bodin, X., Schoeneich, P., Baron, L., and Gardent, M.: The influence of ground ice distribution on geomorphic dynamics since the Little Ice Age in proglacial areas of two cirque glacier systems, Earth Surf. Proc. Land., 40, 666–680, doi:10.1002/esp.3666, 2015.

Carrivick, J. L., Geilhausen, M., Warburton, J., Dickson, N. E., Carver, S. J., Evans, A. J., and Brown, L. E.: Contemporary geomorphological activity throughout the proglacial area of an alpine catchment, Geomorphology, 188, 83–95, doi:10.1016/j.geomorph.2012.03.029, 2013.

Carturan, L., Baldassi, G. A., Bondesan, A., Calligaro, S., Carton, A., Cazorzi, F., Dalla Fontana, G., Francese, R., Guarnieri, A., Milan, N., Moro, D., and Tarolli, P.: Current behaviour and dynamics of the lowermost Italian glacier (Montasio Occidentale, Julian Alps), Geogr. Ann. A, 95, 79–96, doi:10.1111/geoa.12002, 2013.

Cogley, J. G., Hock, R., Rasmussen, L. A., Arendt, A. A., Bauder, A., Braithwaite, R. J., Jansson, P., Kaser, G., Möller, M., Nicholson, L., and Zemp, M.: Glossary of glacier mass balance and related terms, IHP-VII technical documents in hydrology No. 86, IACS Contribution No. 2., 2011.

Conforti, D., Deline, P., Mortara, G., and Tamburini, A.: Terrestrial scanning LiDAR technology applied to study the evolution of the ice-contact Miage lake (Mont Blanc, Italy), Proceedings of the 9th Alpine Glaciological Meeting, Milan, Italy, 2005.

Colucci, R. R., Forte, E., Boccali, C., Dossi, M., Lanza, L., Pipan, M., and Guglielmin, M.: Evaluation of Internal Structure, Volume and Mass of Glacial Bodies by Integrated LiDAR and Ground Penetrating Radar Surveys: The Case Study of Canin Eastern Glacieret (Julian Alps, Italy), Surv. Geophys., 36(2), 231–252, doi:10.1007/s10712-014-9311-1, 2015.

Cox, L. H., and March, R. S.: Comparison of geodetic and glaciological mass-balance techniques, Gulkana Glacier, Alaska, U.S.A, J. Glaciol., 50(170), 363–370, doi:10.3189/172756504781829855, 2004.

Deems, J. S., Painter, T. H., and Finnegan, D. C.: Lidar measurement of snow depth: a review, J. Glaciol., 59(215), 467–479, doi:10.3189/2013JoG12J154, 2013.

Deems, J. S., Gadomski, P. J., Vellone, D., Evanczyk, R., LeWinter, A. L., Birkeland, K. W., and Finnegan, D. C.: Mapping starting zone snow depth with a ground-based lidar to assist avalanche control and forecasting, Cold Reg. Sci. Technol., 120, 197–204, doi:10.1016/j.coldregions.2015.09.002, 2015.

Dyurgerov, M. B.: Glacier mass balance and regime: Data of measurements and analysis, Occasional Paper 55, Institute of Arctic and Alpine Research, University of Colorado, Boulder, CO, 2002.

Egli, L., Jonas, T., Grünewald, T., Schirmer, M., and Burlando, P.: Dynamics of snow ablation in a small Alpine catchment observed by repeated terrestrial laser scans, Hydrol. Process., 26(10), 1574–1585, doi:10.1002/hyp.8244, 2012.

Fischer, A.: Comparison of direct and geodetic mass balances on a multi-annual time scale, The Cryosphere, 5, 107–124, doi:10.5194/tc-5-107-2011, 2011.

Fischer, A., Seiser, B., Stocker Waldhuber, M., Mitterer, C., and Abermann, J.: Tracing glacier changes in Austria from the Little Ice Age to the present using a lidar-based high-resolution glacier inventory in Austria, The Cryosphere, 9, 753–766, doi:10.5194/tc-9-753-2015, 2015a.

Fischer, M., Huss, M., Barboux, C., and Hoelzle, M.: The new Swiss Glacier Inventory SGI2010: Relevance of using high-resolution source data in areas dominated by very small glaciers, Arct., Antarct. Alp. Res., 46(4), 935–947, doi:10.1657/1938-4246.4.935, 2014.

Fischer, M., Huss, M., and Hoelzle, M.: Surface elevation and mass changes of all Swiss glaciers 1980–2010, The Cryosphere, 9, 525-540, doi:10.5194/tc-9-525-2015, 2015b.

Gabbud, C., Micheletti, N., and Lane, S. N.: Lidar measurements of surface melt for a temperate Alpine glacier at the

seasonal and hourly scales, J. Glaciol., 61(229), 963–974, doi:10.3189/2015JoG14J226, 2015.

Gardent, M., Rabatel, A., Dedieu, J.-P., and Deline, P.: Multi-temporal glacier inventory of the French Alps from the late 1960s to the late 2000s, Global Planet. Change, 120, 24–37, doi:10.1016/j.gloplacha.2014.05.004, 2014.

Gilbert, A., Vincent, C., Wagnon, P., Thibert, E., and Rabatel, A.: The influence of snow cover thickness on the thermal regime of Tête Rousse Glacier (Mont Blanc range, 3200 m a.s.l.): Consequences for outburst flood hazards and glacier response to climate change, J. Geophys. Res., 117, F04018, doi:10.1029/2011JF002258, 2012.

Grunewald, K., and Scheithauer, J.: Europe's southernmost glaciers: response and adaptation to climate change, J. Glaciol, 56(195), 129–142, doi:10.3189/002214310791190947, 2010.

Grünewald, T., Schirmer, M., Mott, R., and Lehning, M.: Spatial and temporal variability of snow depth and ablation rates in a small mountain catchment, The Cryosphere, 4, 215–225, doi:10.5194/tc-4-215-2010, 2010.

Haberkorn, A., Phillips, M., Kenner, R., Rhyner, H., Bavay, M., Galos, S. P., and Hoelzle, M.: Thermal regime of rock and its relation to snow cover in steep Alpine rock walls: Gemsstock, central Swiss Alps, Geogr. Ann. A, 97, 579–597, doi:10.1111/geoa.12101, 2015.

Hagg, W., Mayer, C., and Steglich, C.: Glacier changes in the Bavarian Alps from 1989/90 to 2006/07, Z. Gletscherkd. Glazialgeol., 42(1), 37–46, 2008.

Hartzell, P. J., Gadomski, P. J., Glennie, C. L., Finnegan, D. C., and Deems, J. S.: Rigorous error propagation for terrestrial laser scanning with application to snow volume uncertainty, J. Glaciol., 61(230), 1147–1158, doi:10.3189/2015JoG15J031, 2015.

Helfricht, K., Kuhn, M., Keuschnig, M., and Heilig, A.: Lidar snow cover studies on glaciers in the Ötztal Alps (Austria): comparison with snow depths calculated from GPR measurements, The Cryosphere, 8, 41–57, doi:10.5194/tc-8-41-2014, 2014.

Heritage, G., and Large, A.: Laser scanning for the environmental sciences, Wiley, Chichester, 288 p, 2009.

Hock, R.: A distributed temperature-index ice- and snowmelt model including potential direct solar radiation, J. Glaciol., 45(149), 101–111, doi:10.3198/1999JoG45-149-101-111, 1999.

Hubbard, B. P., Hubbard, A., Mader, H. M., Tison, J.-L., Grust, K., and Nienow, P. W.: Spatial variability in the water content and rheology of temperate glaciers: Glacier de Tsanfleuron, Switzerland, Ann. Glaciol., 37(1), 1–6, doi:10.3189/172756403781815474, 2003.

Huss, M.: Mass balance of Pizolgletscher, Geogr. Helv., 65(2), 80–91, doi:10.5194/gh-65-80-2010, 2010.

Huss, M.: Density assumptions for converting geodetic glacier volume change to mass change, The Cryosphere, 7, 877–887, doi:10.5194/tc-7-877-2013, 2013.

Huss, M., and Hock, R.: A new model for global glacier change and sea-level rise, Front. Earth Sci., 3, 54, doi:10.3389/feart.2015.00054, 2015.

Huss, M., and Fischer, M.: Sensitivity of very small glaciers in the Swiss Alps to future climate change, Front. Earth Sci., 4, 34, doi:10.3389/feart.2016.00034, 2016.

Huss, M., Bauder, A., and Funk, M.: Homogenization of long-term mass balance time series, Ann. Glaciol., 50(50), 198–206, doi:10.3189/172756409787769627, 2009.

Huss, M., Dhulst, L., and Bauder, A.: New long-term mass balance series for the Swiss Alps, J. Glaciol., 61(227), 551–562, doi:10.3189/2015JoG15J015, 2015.

Jansson, P.: Effect of uncertainties in measured variables on the calculated mass balance of Storglaciären, Geogr. Ann. A, 81, 633–642, doi:10.1111/1468-0459.00091, 1999.

Joerg, P. C., Morsdorf, F., and Zemp, M.: Uncertainty assessment of multi-temporal airborne laser scanning data: A case study on an Alpine glacier, Remote Sens. Environ., 127, 118–129, doi:10.1016/j.rse.2012.08.012, 2012.

Jost, G., Moore, R. D., Menounos, B., and Wheate, R.: Quantifying the contribution of glacier runoff to streamflow in the upper Columbia River Basin, Canada, Hydrol. Earth Syst. Sci., 16, 849–860, doi:10.5194/hess-16-849-2012, 2012.

Kääb, A., Berthier, E., Nuth, C., Gardelle, J., and Arnaud, Y.: Contrasting patterns of early twenty-first-century glacier mass change in the Himalayas, Nature, 488, 495–498, doi:10.1038/nature11324, 2012.

Kenner, R., Phillips, M., Danioth, C., Denier, C., Thee, P., and Zgraggen, A.: Investigation of rock and ice loss in a recently deglaciated mountain rock wall using terrestrial laser scanning: Gemsstock, Swiss Alps, Cold Reg. Sci. Technol., 67, 157–164, doi:10.1016/j.coldregions.2011.04.006, 2011.

Kronenberg, M., Barandun, M., Hoelzle, M., Huss, M., Farinotti, D., Azisov, E., Usubaliev, R., Gafurov, A., Petrakov, D., and Kääb, A.: Mass balance reconstruction for Glacier No. 354, Tien Shan, from 2003 to 2014, Ann. Glaciol., 57(71), 92–102, doi:10.3189/2016AoG71A032, 2016.

Kuhn, M.: The mass balance of very small glaciers, Z. Gletscherkd. Glazialgeol., 31(1): 171–179, 1995.

Kummert, M., and Delaloye, R.: Quantifying sediment transfer between the front of an active alpine rock glacier and a torrential gully. In: Jasiewicz J., Zwolinski Z., Mitasova H., Hengl T. (eds) (2015) Geomorphometry for Geosciences. Adam Mickiewicz University in Poznan - Institute of Geoecology and Geoinformation, International Society for Geomorphometry, Poznan, pp. 278, 2015.

Lane, S. N., Reid, S. C., Westaway, R. M., and Hicks, D. M.: Remotely sensed topographic data for river channel research: the identification, explanation and management of error. In Kelly, R. E. J., Drake, N. A., and Barr, S. L. (eds): Spatial modelling of the terrestrial environment, John Wiley and Sons, Chichester, 157–174, 2004.

López-Moreno, J. I., Revuelto, J., Rico, I., Chueca-Cía, J., Julián, A., Serreta, A., Serrano, E., Vicente-Serrano, S. M., Azorín-Molina, C., Alonso-González, E., and García-Ruiz, J. M.: Thinning of the Monte Perdido Glacier in the Spanish Pyrenees since 1981, The Cryosphere, 10, 681–694, doi:10.5194/tc-10-681-2016, 2016.

Magnússon, E., Muñoz-Cobo Belart, J., Pálsson, F., Ágústsson, H., and Crochet, P.: Geodetic mass balance record with rigorous uncertainty estimates deduced from aerial photographs and lidar data – Case study from Drangajökull ice cap, NW Iceland, The Cryosphere, 10, 159–177, doi:10.5194/tc-10-159-2016, 2016.

MeteoSwiss: Klimabulletin Jahr 2014, Zurich, 2015.

MeteoSwiss: Klimabulletin Jahr 2015, Zurich, 2016.

Østrem, G., and Brugman, M.: Glacier mass-balance measurements: A manual for field and office work, NHRI Science Report, Saskatoon, Canada, 224 pp., 1991.

Perroy, R. L., Bookhagen, B., Asner, G. P., and Chadwick, O. A.: Comparison of gully erosion estimates using airborne and ground-based LiDAR on Santa Cruz Island, California, Geomorphology, 118, 288–300, doi:10.1016/j.geomorph.2010.01.009, 2010.

Pfeffer, W. T., Arendt, A. A., Bliss, A., Bolch, T., Cogley, J. G., Gardner, A. S., Hagen, J.-O., Hock, R., Kaser, G., Kienholz, C., Miles, E. S., Moholdt, G., Mölg, N., Paul, F., Radić, V., Rastner, P., Raup, B. H., Rich, J., and Sharp, M. J.: The Randolph Glacier Inventory: a globally complete inventory of glaciers, J. Glaciol., 60(221), 537–552, doi:10.3189/2014JoG13J176, 2014.

Piermattei, L., Carturan, L., de Blasi, F., Tarolli, P., Dalla Fontana, G., Vettore, A., and Pfeifer, N.: Analysis of glacial and periglacial processes using structure from motion, Earth Surf. Dynam. Discuss., 3, 1345–1398, doi:10.5194/esurfd-3-1345-2015, 2015a.

Piermattei, L., Carturan, L., and Guarnieri, A.: Use of terrestrial photogrammetry based on structure-from-motion for mass balance estimation of a small glacier in the Italian alps, Earth Surf. Proc. Land., 40(13), 1791–1802, doi: 10.1002/esp.3756, 2015b.

Prokop, A., and Panholzer, H.: Assessing the capability of terrestrial laser scanning for monitoring slow moving landslides, Nat. Hazards Earth Syst. Sci., 9, 1921–1928, doi:10.5194/nhess-9-1921-2009, 2009.

Prokop, A., Schirmer, M., Rub, M., Lehning, M., and Stocker, M.: A comparison of measurement methods: terrestrial laser scanning, tachymetry and snow probing for the determination of the spatial snow-depth distribution on slopes, Ann. Glaciol., 49(1), 210–216, doi:10.3189/172756408787814726, 2008.

Rabatel, A., Deline, P., Jaillet, S., and Ravanel, L.: Rock falls in high-alpine rock walls quantified by terrestrial LiDAR measurements: a case study in the Mont Blanc area, Geophys. Res. Lett., 35, L10502, doi:10.1029/2008GL033424, 2008.

Ravanel, L., Bodin, X., and Deline, P.: Using Terrestrial Laser Scanning for the Recognition and Promotion of High-Alpine Geomorphosites, Geoheritage, 6(2), 129–140, doi:10.1007/s12371-014-0104-1, 2014.

Rieger, P., and Ullrich, A.: Resolving range ambiguities in high-repetition rate airborne light detection and ranging applications, J. Appl. Remote Sens., 6(1), 063552–1, doi:10.1117/1.JRS.6.063552, 2012.

RIEGL Laser Measurement Systems: Instruction Manual - *Riegl* VZ-6000 Safety Guidelines, RIEGL Laser Measurement Systems, Horn, Austria, 2012.

RIEGL Laser Measurement Systems: Preliminary Data Sheet, 07.05.2013; *Riegl* VZ-6000 - 3D Ultra long range terrestrial laser scanner with online waveform processing, RIEGL Laser Measurement Systems, Horn, Austria, 2013.

RIEGL Laser Measurement Systems: RiSCAN PRO® – Version 2.1.1, Riegl Laser Measurement Systems, Horn, Austria, 2015.

Rignot, E., Rivera, A., and Casassa, G.: Contribution of the Patagonia Icefields of South America to sea level rise, Science, 302, 434–437, doi:10.1126/science.1087393, 2003.

Rolstad, C., Haug, T., and Denby, B.: Spatially integrated geodetic glacier mass balance and its uncertainty based on geostatistical analysis: application to the western Svartisen ice cap, Norway, J. Glaciol., 55(192), 666–680, doi:10.3189/002214309789470950, 2009.

Schiefer, E., Menounos, B., and Wheate, R.: Recent volume loss of British Columbian glaciers, Canada, Geophys. Res. Lett., 34, L16503, doi:10.1029/2007GL030780, 2007.

Schürch, P., Densmore, A. L., Rosser, N. J., Lim, M., and McArdell, B. W.: Detection of surface change in complex topography using terrestrial laser scanning: application to the Illgraben debris-flow channel, Earth Surf. Proc. Land., 36, 1847–1859, 10.1002/esp.2206, 2011.

Schwalbe, E., Maas, H. G., Dietrich, R., and Ewert, H.: Glacier velocity determination from multi temporal terrestrial long range laser scanner point clouds, The International Archives of the Photogrammetry, Remote Sensensing and Spatial Information Sciences, 37, 457–462, 2008.

Smiraglia, C., Azzoni, R. S., D'Agata, C., Maragno, D., Fugazza, D., and Diolaiuti, G. A.: The evolution of the Italian glaciers from the previous data base to the new Italian inventory, preliminary considerations and results, Geogr. Fis. Dinam. Quat., 38(1), 79–87,2015.

Sold, L., Huss, M., Hoelzle, M., Andereggen, H., Joerg, P. C., and Zemp, M.: Methodological approaches to infer end-of-winter snow distribution on alpine glaciers, J. Glaciol., 59(218), 1047–1059, doi:10.3189/2013JoG13J015, 2013.

Sold, L., Huss, M., Eichler, A., Schwikowski, M., and Hoelzle, M.: Unlocking annual firn layer water equivalents from ground-penetrating radar data on an Alpine glacier, The Cryosphere, 9, 1075–1087, doi:10.5194/tc-9-1075-2015, 2015.

Sold, L., Huss, M., Machguth, H., Joerg, P. C., Leysinger Vieli, G., Linsbauer, A., Salzmann, N., Zemp, M., and Hoelzle, M.: Mass balance reanalysis of Findelengletscher, Switzerland; benefits from extensive snow accumulation measurements, Front. Earth Sci, 4, 18, doi:10.3389/feart.2016.00018, 2016.

Thibert, E., Blanc, R., Vincent, C., and Eckert, N.: Glaciological and volumetric mass balance measurements error analysis over 51 years for the Sarennes glacier, French Alps, J. Glaciol., 54(186), 522–532, doi:10.3189/002214308785837093, 2008.

Tolle, F., Prokop, A., Bernard, É., Friedt, J.-M., and Griselin, M.: Terrestrial laser scanning as a tool to evaluate the quality of interpolated ablation stakes data and the uncertainty of an Arctic glacier mass balance, Abstract C21F-02 presented at 2015 Fall Meeting, AGU, San Francisco, Calif., 14-18 Dec., 2015.

Vincent, C., Kappenberger, G., Valla, F., Bauder, A., Funk, M., and Le Meur, E.: Ice ablation as evidence of climate change in the Alps over the 20th century, J. Geophys. Res., 109, D10104, doi:10.1029/2003JD003857, 2004.

WGMS (World Glacier Monitoring Service): Fluctuations of Glaciers 2005–2010 (Vol. X), edited by: Zemp, M., Frey, H., Gärtner-Roer, I., Nussbaumer, S. U., Hoelzle, M., Paul, F., and Haeberli, W., ICSU (WDS)/IUGG (IACS)/UNEP/UNESCO/WMO, World Glacier Monitoring Service, Zurich, Switzerland, 336 pp., publication based on database version: doi:10.5904/wgms-fog-2012-11, 2012.

WGMS (World Glacier Monitoring Service): Glacier Mass Balance Bulletin No. 12 (2010-2011), edited by: Zemp, M., Nussbaumer, S. U., Naegeli, K., Gärtner-Roer, I., Paul, F., Hoelzle, M., and Haeberli, W., ICSU (WDS)/IUGG (IACS)/UNEP/UNESCO/WMO, World Glacier Monitoring Ser-

vice, Zurich, Switzerland, 106 pp., publication based on database version: doi:10.5904/wgms-fog-2013-11, 2013.

Zhang, Z.: Iterative point matching for registration of ree-form curves, Int. J. Comput. Vision, 13, 119–152, doi:10.1007/BF01427149, 1992.

Zemp, M., Haeberli, W., Hoelzle, M., and Paul, F.: Alpine glaciers to disappear within decades?, Geophys. Res. Lett., 33, L13504, doi:10.1029/2006GL026319, 2006.

Zemp, M., Thibert, E., Huss, M., Stumm, D., Rolstad Denby, C., Nuth, C., Nussbaumer, S. U., Moholdt, G., Mercer, A., Mayer, C., Joerg, P. C., Jansson, P., Hynek, B., Fischer, A., Escher-Vetter, H., Elvehøy, H., and Andreassen, L. M.: Reanalysing glacier mass balance measurement series, The Cryosphere, 7, 1227–1245, doi:10.5194/tc-7-1227-2013, 2013.